SUPPLEMENTARY METHODS

SERRS nanostar physicochemical characterization

For characterization by transmission electron microscopy, a sample of SERRS nanostars was put on a carbon film coated-copper grid (300 Mesh, Electron Microscopy Sciences) and air-dried. Images were typically acquired at magnification factors ranging from 25,000× to 500,000× using a JEOL 1200EX (JEOL USA, Inc.) operated at 80 kV. Images were analyzed with Fiji software [Fiji Is Just ImageJ, http://fiji.sc] to measure the size of the gold core and thickness of the silica shell. The hydrodynamic diameter of equimolar amounts of bare gold nanostars, SERRS nanostars, and PEGylated SERRS nanostars was determined by nanoparticle tracking analysis (NanoSight NS500, Malvern Instruments), which relates the Brownian motion to particle size. The rate of movement is related only to the viscosity of the liquid and the temperature and size of the particle, and is not influenced by particle density or refractive index.

The zeta potential of bare gold nanostars, SERRS nanostars, and PEGylated SERRS nanostars (10 pM at pH 7.4) was measured on a Zetasizer Nano ZS (Malvern Instruments). Absorption spectra of 0.2 nM suspensions of bare gold nanostars, SERRS nanostars, and PEGylated SERRS nanostars in ultrapure water were measured on an Infinite M1000 Pro microplate reader (Tecan Group Ltd.) in a range of 400 – 800 nm with increments of 5 nm.

Limit of detection of SERRS nanostars

The limit of detection was determined by serially diluting 10 pM of SERRS nanostars in solution resulting in a final concentration range of 0.16 fM – 10 pM. Raman images of the phantom were acquired (100 mW, 1.5 s acquisition time, 5× objective) and the signals quantified with Fiji software.

Batch-to-batch reproducibility and stability

To determine batch-to-batch consistency, the Raman intensity of the 950 cm^{-1} peak in the spectrum of IR-780 perchlorate was measured in 3 different batches of 1.0 nM SERRS nanostar preparations. In addition, the size distribution and nanoparticle concentration of as-synthesized non-PEGylated SERRS nanostars were determined by nanoparticle tracking analysis. Typical concentrations ranged between 3 nM and 5 nM of as-synthesized SERRS nanostars, which were stored until injection as 3.5 nM preparations in 10 mM MES buffer (pH 7.3).

The photostability of SERRS nanostars was determined by irradiating a 1.0-nM SERRS nanostar suspension for 25 minutes at 100 mW laser power. A Raman spectrum was acquired from the SERRS nanostars (50 μW laser power, 1.0 s acquisition time, 5× objective) every 5 min during continuous laser irradiation. Serum stability of 1.0 nM SERRS nanostars was assessed in 50% mouse serum (AbD Serotec) in a total volume of 100 μl. SERRS signal intensity and hydrodynamic diameter were determined at 0, 4, 8, 18, 24, 48, and 72 hours.

Biodistribution in wild-type mice

Eight-week-old wild-type C57BL/6NCrl mice (n = 10) were purchased from Charles River Laboratories. The mice were injected with 30 fmol/g PEGylated SERRS nanostars and euthanized 16–18 hours later using CO_2 asphyxiation. In one set of mice (n = 5) organs were harvested, weighed, and homogenized. Tissue homogenates were placed in 384-well plates; Raman images of the plates were acquired at 10 mW, 1.5 s acquisition time, 5× objective. In a second set of mice (n = 5) the gastrointestinal tracts from the stomach to the rectum were excised and Raman images of the intact tracts acquired ex vivo (same imaging parameters).

Generation of mouse models of human breast cancer, sarcoma, pancreatic cancer, and prostate cancer

The MMTV-PyMT female mice (FVB/N-Tg(*MMTV-PyVT*)634Mul/J) express the polyoma virus middle T antigen under the direction of the mouse mammary tumor virus promoter/enhancer (*18*). The dedifferentiated liposarcoma model was generated by subcutaneous injection of 1×10^6 DDLS8817 human liposarcoma cells into the flank of 8-week-old NOD/Shi-*SCID*/*Il2rγ*$^{-/-}$ (NOG) male mice (Taconic) (*43*). *Nestin-tv-a*; *Ink4a*/*Arf*$^{-/-}$; *Pten*$^{fl/fl}$ (abbreviated as *Ink4a*/*Arf*$^{-/-}$) mice are particularly susceptible to developing soft-tissue sarcomas due to loss of *Ink4a*, which arise in the subcutis and invade the underlying musculature (*17, 44*). Without the presence of Cre, the floxed *Pten* allele is intact and functional as wild type. In addition, *tv-a* alone (an avian-specific retroviral receptor), driven by the *Nestin* gene promoter, has no effect on tumorigenesis. The *LSL-Kras*$^{G12D/+}$*; LSL-Trp53*$^{R172H/+}$*; Pdx-1-Cre* (or KPC) model is a well-validated, clinically relevant model of PDAC (*15*). KPC mice develop a spectrum of premalignant lesions that ultimately progress to overt pancreatic ductal adenocarcinoma with 100% penetrance. The Hi-Myc transgenic mouse model (*16*) uses the modified *ARR2*/*Pbsn* promoter to overexpress human MYC in the mouse prostate. These mice develop PIN lesions as early as 2 weeks, which progress to invasive carcinoma by 6 to 9 months and share several similarities with the human disease.

***In vitro* cellular uptake studies of SERRS nanostars**

AT-3 cells [established from a primary mammary carcinoma of the MMTV-PyMT transgenic mouse model (*22*)], DDLS8817 cells [derived from a human liposarcoma (*19*)], PCC-9 cells [derived from the KPC mouse pancreatic cancer (*23*)], and Myc-CaP cells [derived from a Hi-Myc transgenic mouse prostate cancer (*24*)] were cultured in DMEM (high glucose) medium with 10% fetal bovine serum, 2 mM L-glutamine and 1 mM sodium pyruvate (Life Technologies) at 37 °C in 5% CO_2.

Cells were seeded into 12-well-plates and treated when they reached 70-80% confluence. Cells were preincubated for 30 min with different macropinocytosis inhibitors, including EIPA (75 μM, Sigma), wortmannin (100 ng/mL, Sigma), NVP-BEZ235 (2 μM, Cayman Chemical) and cytochalasin D (10 μg/mL, MP Biomedicals) in dimethylsulfoxide (DMSO). The concentrations used were based on prior literature (*21*). Then, SERRS nanostars were added to the culture medium at a final concentration of 2 pM and cells were incubated for 3 hours. Finally, cells were trypsinized, rinsed 3× with PBS and seeded into 384-well-plates for Raman imaging (10 mW laser power, 1.5 s acquisition time, 5× objective). A Raman map was generated by using a direct classical least squares algorithm (Wire 3.4 software, Renishaw). An aliquot from each sample was used for counting of cell numbers and the total uptake was normalized to the cell number. The mean values and standard deviations of inhibition effects by different inhibitors, normalized to DMSO-treated sample, were calculated. All experiments were run in triplicate.

SUPPLEMENTARY FIGURES

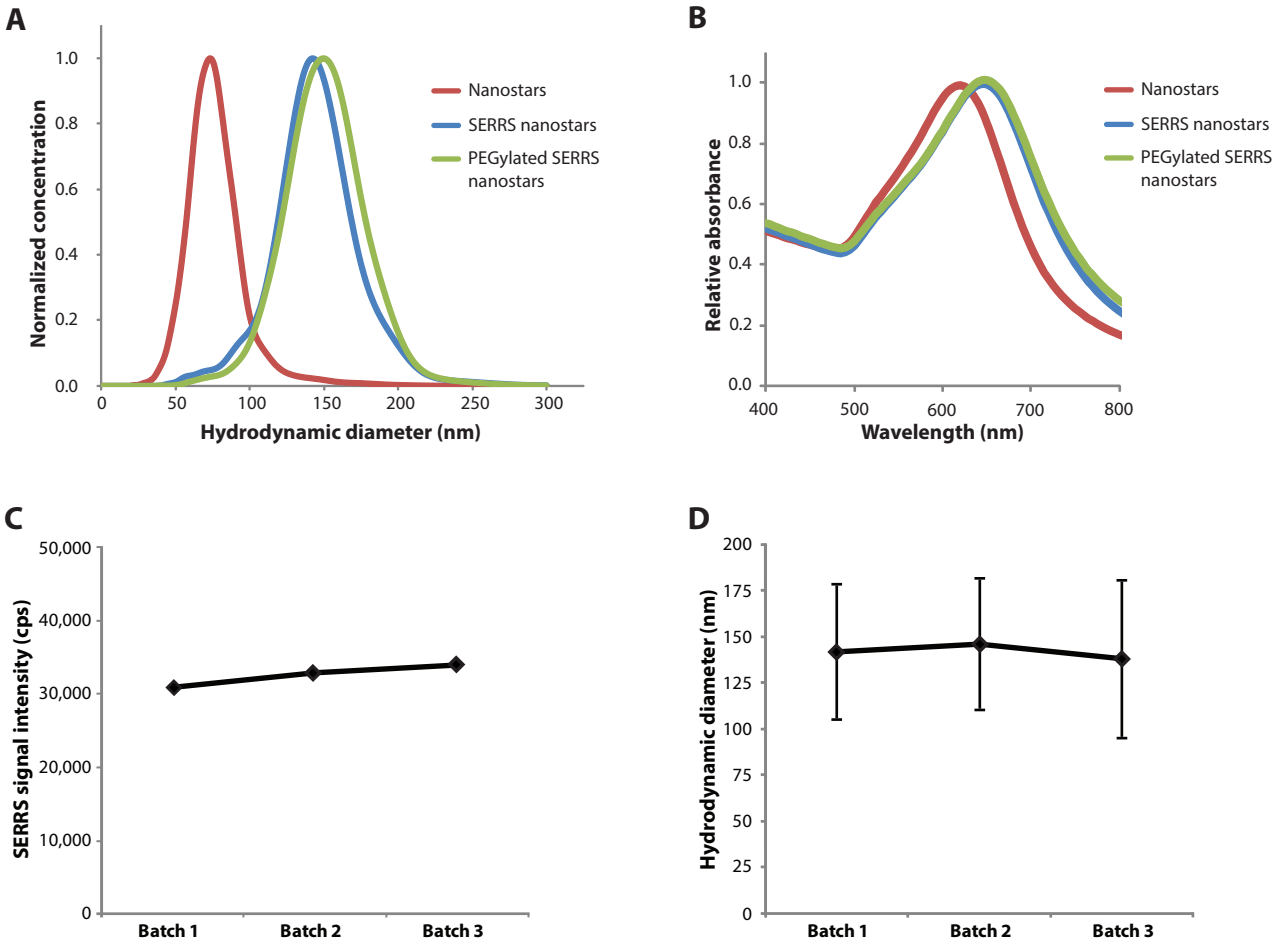

Figure S1. Characterization of SERRS nanostars. (**A**) The hydrodynamic size distribution of bare gold nanostars (75 nm), SERRS nanostars (142 nm), and PEGylated SERRS nanostars (150 nm) was measured by nanoparticle tracking analysis. (**B**) Absorption spectra of equimolar amounts of gold nanostars, SERRS nanostars, and PEGylated SERRS nanostars. (**C**) Signal intensity of the 950 cm^{-1} peak was measured in 3 different batches. The signal intensity of 1.0 nM SERRS nanostars at 50 µW (1.0 s acquisition time, 5× objective) was 32583 ± 1479 (mean ± SD) counts per second. (**D**) The size distribution of 3 different batches of 1.0 pM SERRS nanostars was measured by nanoparticle tracking analysis. Data represent the mean hydrodynamic diameter and error bars the size variation (± SD) within a population of SERRS nanostars for each batch.

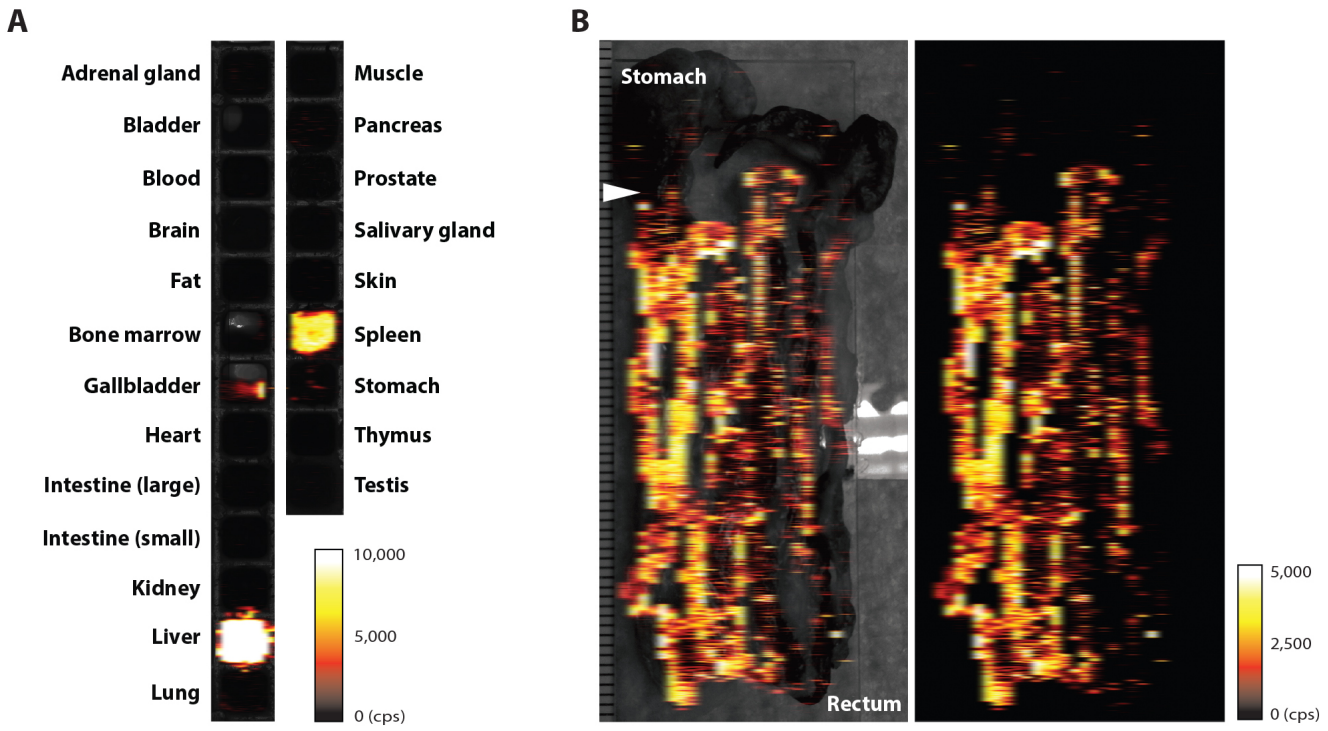

Figure S2. Tissue distribution and biliary excretion of SERRS nanostars. (**A**) C57BL/6 mice were injected intravenously with SERRS nanostars (30 fmol/g). Organs were harvested 16 h later (intestinal contents were mechanically removed) and homogenized tissues analyzed by Raman imaging (10 mW, 1.5 s acquisition time, 5× objective) to determine the relative accumulation in different tissues. Images are Raman/white light overlays and representative of $n = 5$ mice, 1 organ per well. SERRS signal intensity is displayed in counts per second (cps). (**B**) The gastrointestinal tracts (stomach to rectum) of C57BL/6 mice ($n = 5$) were excised 16 hours after intravenous injection of SERRS nanostars and Raman images were acquired (10 mW, 1.5 s acquisition time, 5× objective). Left: Raman/white light image overlay. Right: Raman image. Arrowhead indicates entry point of the common bile duct into the small bowel. SERRS signal intensity is displayed in cps.

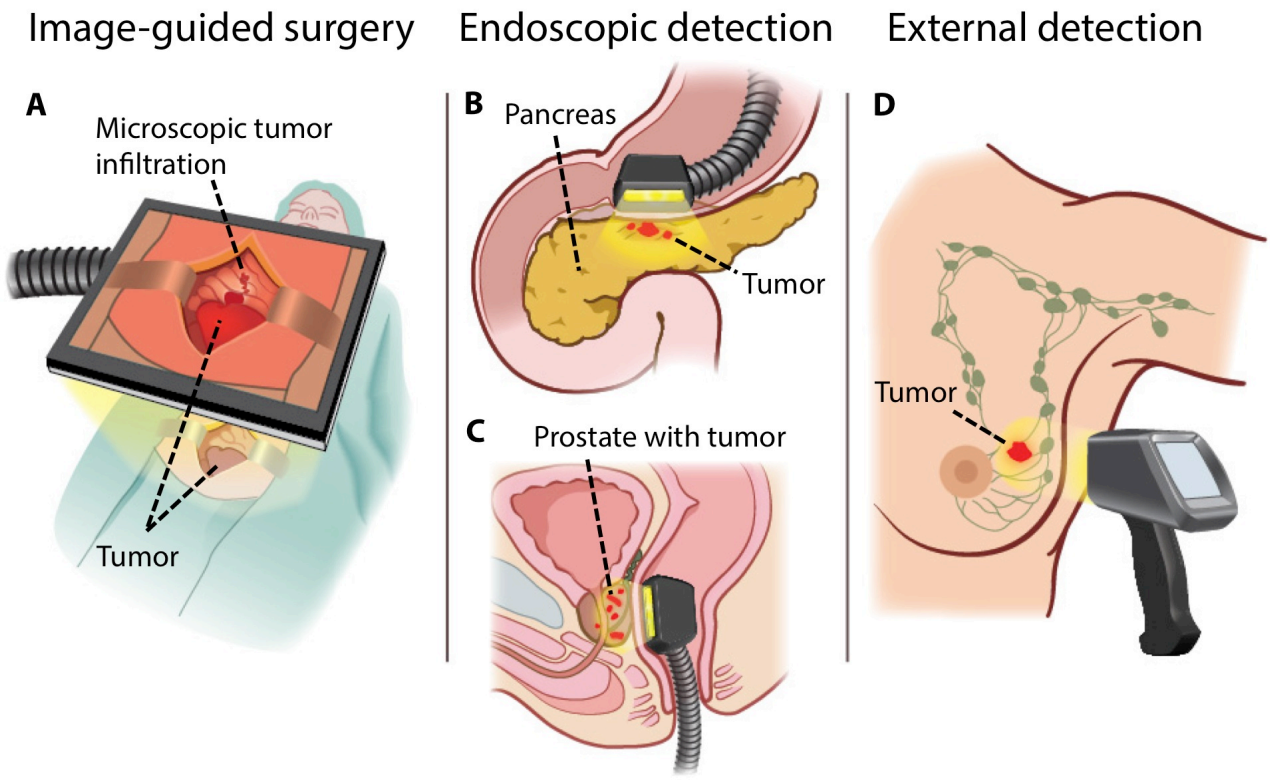

Figure S3. Potential clinical applications of SERRS nanostars. (A) Rapid wide-field Raman imaging systems [currently in development (*12*)] could be used in the operating room to better visualize tumor margins, microscopic tumor infiltrations, and loco-regional metastases. (**B** and **C**) Raman deep-tissue imaging endoscopes using surface-enhanced spatially offset Raman spectroscopy (SESORS) technology (*41*) could be used for image-guided tumor detection and intervention for e.g. pancreas (B) or prostate (C) cancers. (**D**) Relatively superficial cancer types, such as breast cancer, could be detected through the skin with SESORS detectors.

SUPPLEMENTARY TABLE

Table S1. Zeta potentials of nanostars. Bare gold nanostars, SERRS nanostars, and PEGylated SERRS nanostars were analyzed at a concentration of 10 pM at pH 7.4. Data represent mean ± SD (*n* = 3).

Type of nanostars	ζ (mV)
Gold nanostars	-48.1 ± 14.2
SERRS nanostars	-48.7 ± 6.44
PEGylated SERRS nanostars	-45.4 ± 11.4